Thermal Fatigue Life Prediction of Glidcop® Al-15

Viswanath Ravindranath, Sushil Sharma, Brian Rusthoven
APS, Argonne National Laboratory, 9700 S. Cass Ave., Argonne, IL 60439, USA
Michael Gosz
Illinois Institute of Technology, 3300 S. Federal St., Chicago, IL 60616, USA
Lin Zhang, Jean-Claude Biasci
ESRF, BP-220, 6, rue Jules Horowitz, 38043 Grenoble Cedex 09, France

Abstract

Photon absorbers, masks, and shutters of the third-generation light sources are subjected to intense thermal stress cycles from the high intensity x-ray beams. A collaborative research study is underway at APS and ESRF to establish thermal fatigue design criteria for Glidcop® Al-15, which is commonly used for high-heat-load components. A nonlinear finite element methodology is used for modeling the nonlinear multiaxial stress-strain behavior of Glidcop test specimens. The methodology consists of transient thermal analyses followed by elastic-plastic analyses that include a creep model. A Socie-modified Smith-Watson-Topper model is used for thermal fatigue life predictions. A good correlation is observed between the predicted thermal fatigue life and experimental observations from thermal cyclic tests at ESRF; these data are presented in detail in a separate paper.

***Keywords**: Thermal fatigue, Nonlinear FEA, SWT fatigue life prediction, Creep, Hold time*

1. Background

The Advanced Photon Source (APS) and the European Synchrotron Research Facility (ESRF) are third-generation light sources that were built to generate extremely powerful x-rays. Many critical components such as photon absorbers, masks, and shutters are used at both facilities to control the exposure of downstream components to the intense x-rays. These components are water cooled and are usually made from Glidcop Al-15, a dispersion-strengthened copper containing 0.15% of submicroscopic alumina particles. Glidcop Al-15 has significantly higher yield strength, ultimate tensile strength, fatigue strength, and rupture strength at elevated temperatures in comparison to OFHC (Oxygen-Free High Conductivity) copper. The thermal conductivity of Glidcop Al-15 is comparable to that of OFHC copper, making it an excellent material for high-heat-load applications.

The following design guidelines have been used for the design of Glidcop components subjected to the intense cyclic heat loads of the x-ray beams:

1) The maximum surface temperature, which occurs at the center of the beam footprint, is not to exceed 300 ºC [1].

2) The maximum von Mises stress in the component should not exceed its yield strength at room temperature.

These design guidelines are too conservative for the expected low number of thermal cycles experienced by most of the components (~10,000 cycles, equivalent to 30 years of service). A collaborative research study was undertaken at APS and ESRF aimed at establishing new design guidelines based on the low-cycle thermal fatigue life of Glidcop Al-15. The new guidelines are expected to reduce the cost of machine upgrades for higher beam current operations planned at both facilities.

2. Experimental Setups at ESRF and APS

As the first part of this research study, a thermal fatigue experiment was carried out at ESRF. In this experiment, four rectangular water-cooled Glidcop Al-15 samples were exposed to an x-ray beam in a cyclic manner. As shown in Fig. 1, the samples measuring 101.6 mm × 22.2 mm × 25.4 mm, were moved vertically by a stepper motor resulting in a 30-second beam exposure per sample. The travel time between two adjacent samples was two seconds. The total power absorbed by the samples was about 1250 W at 200 mA of beam current and a beam size of 4.2 mm × 4.2 mm. The maximum temperature seen by the samples as a result of the beam exposure was 604 °C.

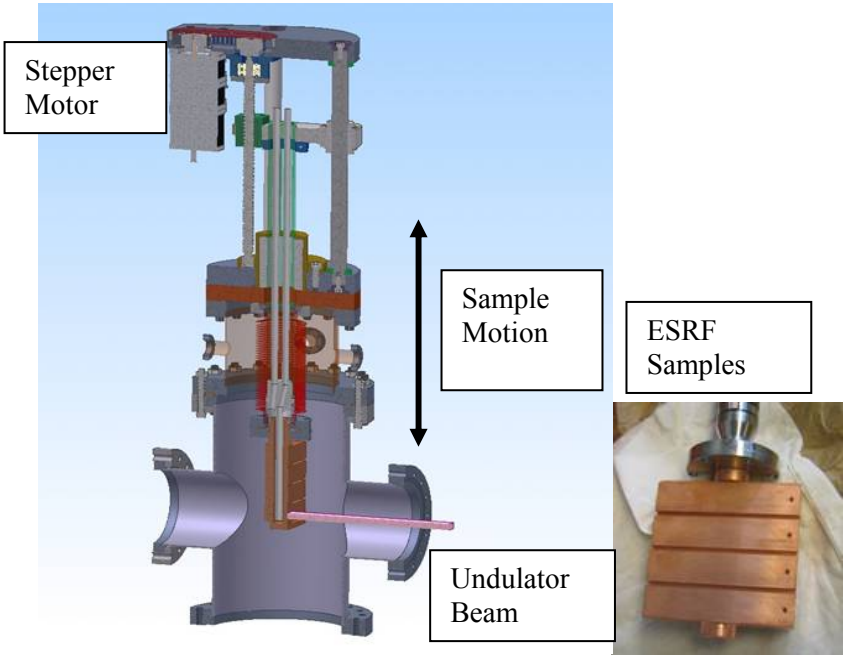

Fig. 1: Thermal fatigue experimental setup at ESRF.

In this study, it was observed that, as a result of thermal cycling at 600 °C for ~15,000 cycles, multiple surface cracks had developed. The cracks had formed not only in the areas that were exposed to beam, but also along the path traversed by the beam including the grooves between the samples. An optical microscopy of the fractured surface revealed that a single dominant crack had penetrated ~1 mm deep in three of the four samples, as shown in Fig. 2. The details of this experimental work are presented in a separate paper [2].

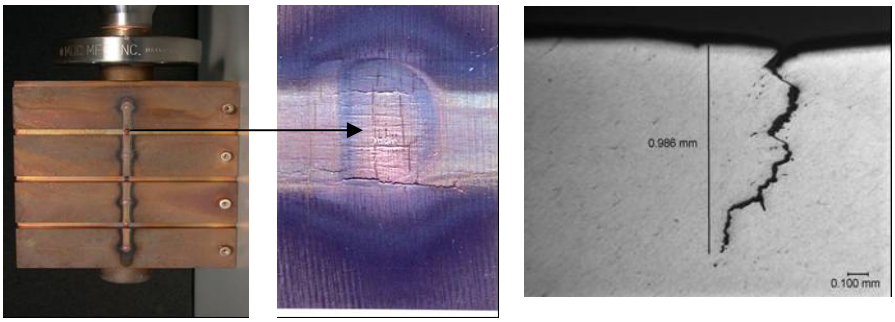

Fig. 2: Thermal fatigue cracks in a Glidcop Al-15 sample tested at ESRF.

As the second part of the research study, further thermal fatigue tests are being carried out at APS with a modified experimental setup. The major differences between this experimental setup and the one that was used at ESRF are as follows:

1) An upstream shutter is being used at APS (Fig. 3) with an electromagnetic actuator that controls the 30-second beam exposure on a specific sample for thermal cycling. The samples do not move until beam exposure cycles on the selected sample have been completed.

2) The cooling water in the APS samples flows through an OFHC copper tube that is brazed to the samples. This was done as a precaution against thermal cracks penetrating into the water channel.

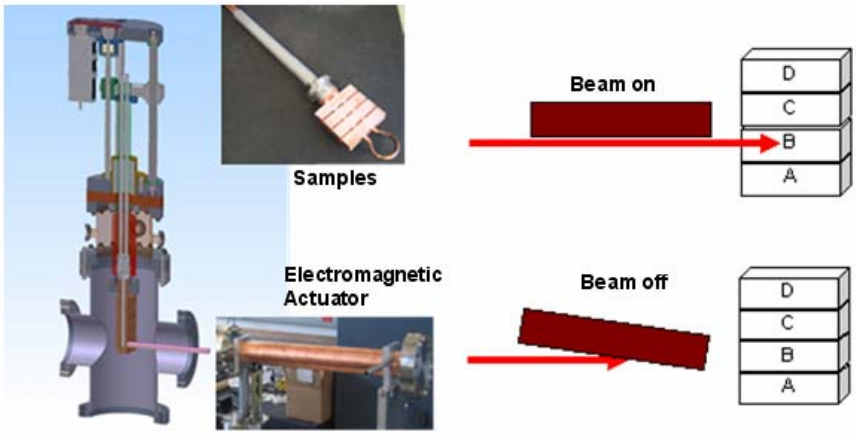

Fig. 3: Thermal fatigue experimental setup at APS.

This experiment at APS is currently being carried out in the sector 26-ID beamline, which receives x-ray beam from two inline undulators (Undulator A). Relevant parameters for this undulator are shown in Table 1.

Table 1: Parameters of the APS Undulator-A [3]

Parameters	**Value**
Beam current	100 mA
Relativistic gamma	13700
Number of periods	144
Undulator parameters	Period length 3.3 cm, undulator length 2.4 m, undulator gap 11 mm
Horizontal beam size, σ_x	0.275 mm
Vertical beam size σ_y	0.009 mm
Horizontal beam divergence σ_x'	0.0113 rad
Vertical Beam divergence σ_y'	0.003 rad

At present there is no direct measurement of the maximum temperature at the center of the beam footprint. However, undulator gaps were selected [4] to achieve predicted temperatures of 600 °C, 550 °C, and 500 °C based on the following considerations: (a) a 2 mm × 2 mm exit mask at 25 m distance from the source limits the beam size to 2.8 mm × 2.8 mm on the sample at 35 m, and (b) because of scattering, only 80% of the beam power is absorbed by the samples. The results of peak temperatures versus undulator gaps are summarized in Table 2. Currently tests are underway to verify the peak temperatures with an infrared camera.

Table 2: Undulator Gaps and Beam Power Corresponding to Estimated Test Temperatures

Expected Test Temperature (°C)	**Absorbed Power (W)**	**Adjusted Power for 20% Scattering (W)**	**Undulator gap (mm)**
600	986	1183	14.3
550	904	1085	15.1
500	823	987	15.6

The thermal cycles at APS are stopped intermittently to visually inspect the test sample for surface cracks with the aid of a high-magnification survey alignment scope. The pictures of the sample's surfaces after various numbers of thermal cycles are shown in Fig. 4.

At the test temperatures, the thermal stresses in the beam footprint region are substantially higher than the yield strength of Glidcop. Local plastic deformations in this region eventually result in thermal fatigue cracks. A nonlinear finite element methodology, discussed in the following section, was used to estimate the cyclic stress and strain fields with nonlinear temperature-dependent material properties.

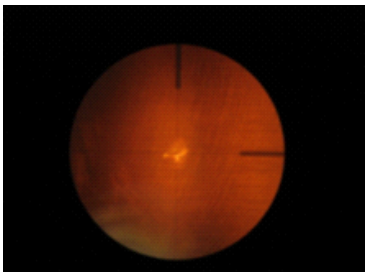

Temperature - 600 °C
Cycles = 4592, Sample #A

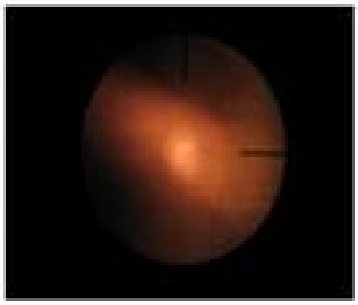

Temperature - 500 °C
Cycles = 1347, Sample #C

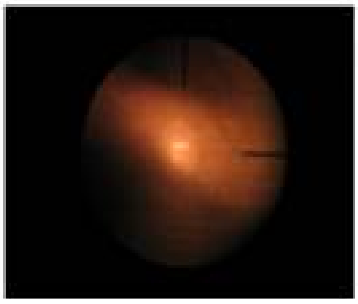

Temperature - 500 °C
Cycles = 3534, Sample #C

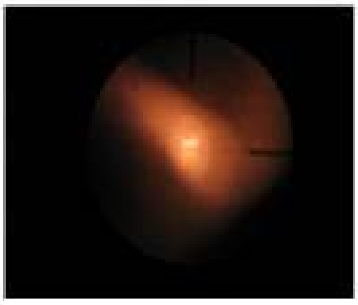

Temperature - 500 °C
Cycles = 5658, Sample #C

Fig. 4: Visual inspection of the APS samples after thermal cycling.

3. Nonlinear Finite Element Methodology

3.1 Finite Element Modeling

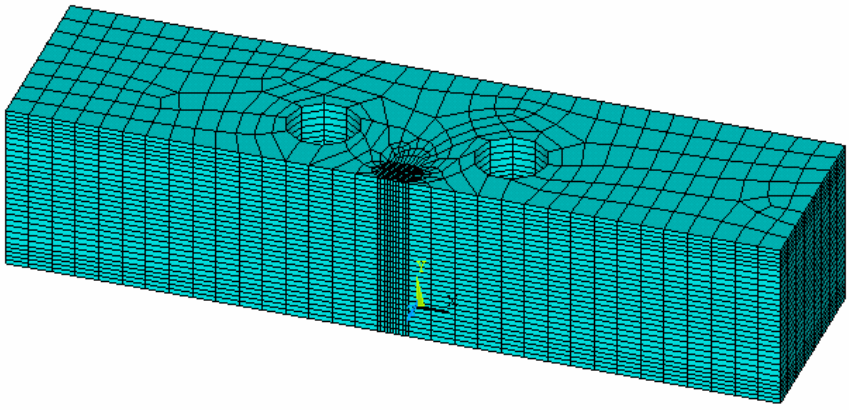

Fig. 5: Finite element mesh of the Glidcop Al-15 test sample.

All finite element (FE) modeling was done with the ANSYS® finite element code. As shown in Fig. 5, a refined mesh density was generated in the region exposed to the x-ray beam. The same mesh configuration, with a total of 12,000 elements, was used for both the thermal and stress analyses with "Solid90" and "Solid186" elements [5], respectively.

3.2 Transient Thermal Analysis

In the transient thermal analysis the heat flux boundary condition was applied in the form of a uniform heat flux over an area of 2.8 mm × 2.8 mm. The uniform nodal heat flux values were computed by dividing the predetermined absorbed heat power corresponding to the estimated temperatures of 600 ºC, 550 ºC, and 500 ºC, as shown in Table 2. The heat transfer film coefficient on the surface of the cooling channel was assumed to be 0.015 W/mm^2-ºC at a bulk reference temperature of 25.6 ºC. Material properties of Glidcop Al-15 for the thermal analysis are shown Table 3.

Table 3: Thermo-Mechanical Properties of Glidcop Al-15 [6]

Parameters	**Glidcop Al-15 (flat plate up to 10 mm thick)**
Thermal conductivity, W/(m-K) @ 293 K	365
Specific heat, J/kg-K	390
Density, Mg/m3	8.90

The evolution of temperature field as a function of time at the center of the x-ray beam footprint is shown in Fig. 6. This transient temperature distribution in the thermal model was then used as the input boundary condition for the subsequent nonlinear stress analysis.

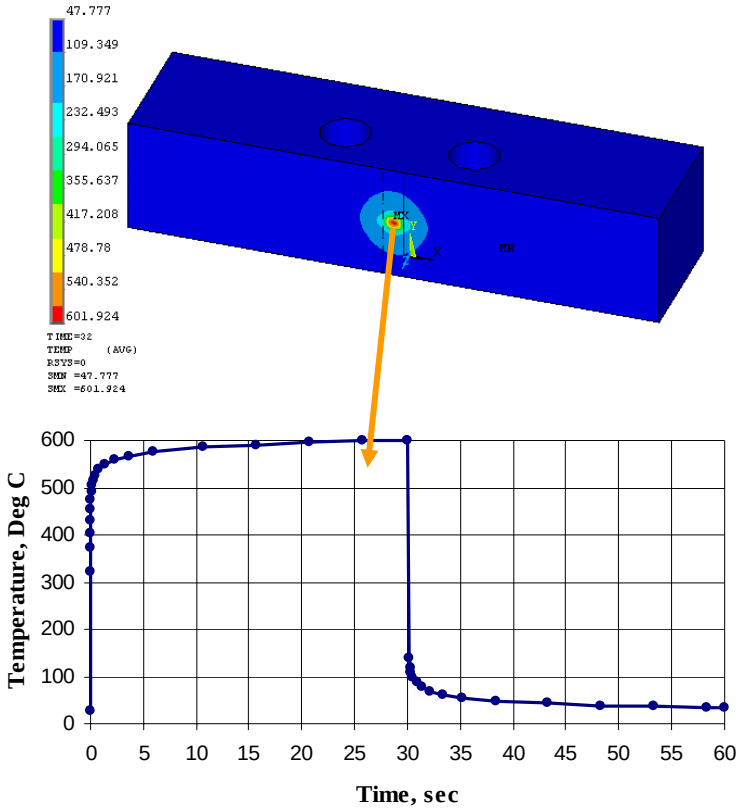

Fig. 6: Evolution of temperature field in the test sample A as a function of time.

3.3 Nonlinear FE Stress Analysis

The nonlinearity in the FE stress analyses is primarily due to the temperature-dependent nonlinear material properties of Glidcop in the plastic range. Because of small deformations, a linear relationship between strain ε_{ij} and nodal displacements u_i was used:

$$\varepsilon_{ij} = \frac{1}{2}\left(u_{i,j} + u_{j,i}\right). \tag{1}$$

It was assumed that the material yields according to von Mises's yield criteria, which is the most commonly used yield criteria for ductile materials. In order to model the cyclic elastic-plastic behavior of a material, one of the main requirements is to define the "hardening" rule, which describes how the yield stress evolves as a function of plastic straining and temperature. For metals such as dispersion-strengthened copper that are cyclically stable [7], the monotonic stress-strain behavior adequately describes their cyclic response [8].

To obtain this monotonic stress-strain data for Glidcop Al-15, tensile tests were carried out on standard tensile Glidcop Al-15 specimens of 0.5 inches diameter at the mechanical testing laboratory at the Illinois Institute of Technology. The stress-strain plots obtained from these tests are shown in Fig. 7. A bilinear kinematic hardening rule, based on the data and obtained from the elevated tensile tests and by interpolating for intermediate temperatures, was used.

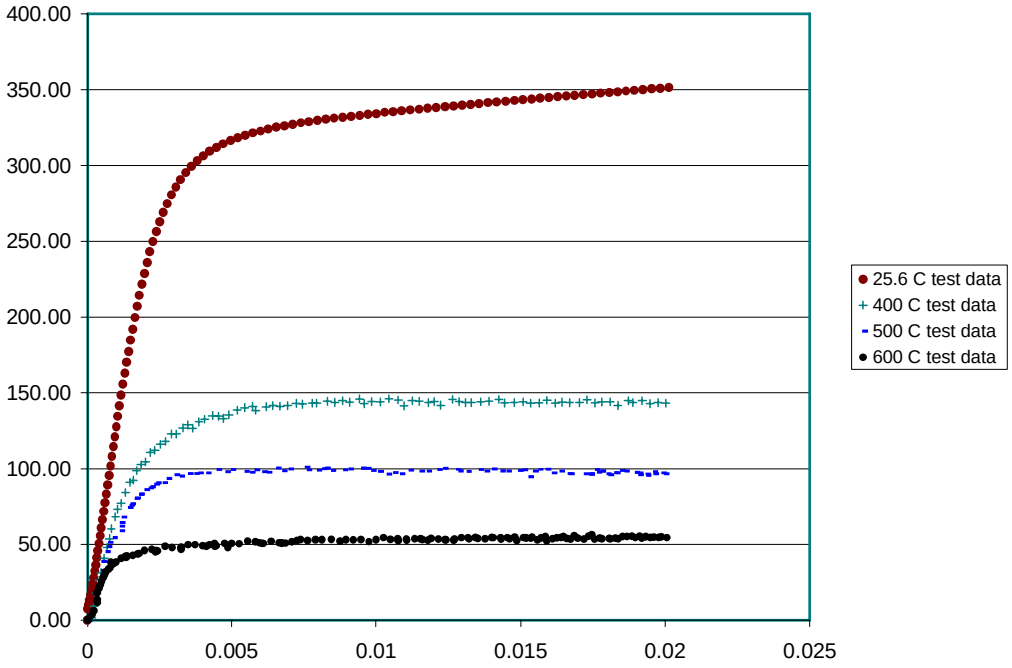

Fig. 7: Stress strain plots at elevated temperature.

The load inputs to the stress analysis are the temperatures calculated in the thermal analysis at the various time steps. Because nonlinear stress analyses are time consuming, only three cycles of thermal loading were considered for simulation.

The results of these nonlinear simulations are shown in Fig. 8 in blue and red hysteresis plots for the maximum test temperatures of 500 °C and 600 °C, respectively. These plots show maximum stress in

the y-direction versus maximum total strain in the x-direction at the center of the beam footprint where maximum plasticity occurs. The hottest region in the specimen is constrained from expanding freely by the surrounding cold region (see Fig. 9), thus resulting in compressive stresses as shown by the line segment O-A-B (Fig. 8) for the Sample A.

Thermal stresses at point A (Fig. 8) exceed yield stress of the material, resulting in localized plastic flow. Since the yield stress decreases with increase in temperature, the branch A-B has a negative slope. During beam-off condition, stresses in the hot central zone reverse direction, becoming tensile. When the tensile stresses exceed the yield point, reverse plastic flow occurs, as shown by the curve B-C-D.

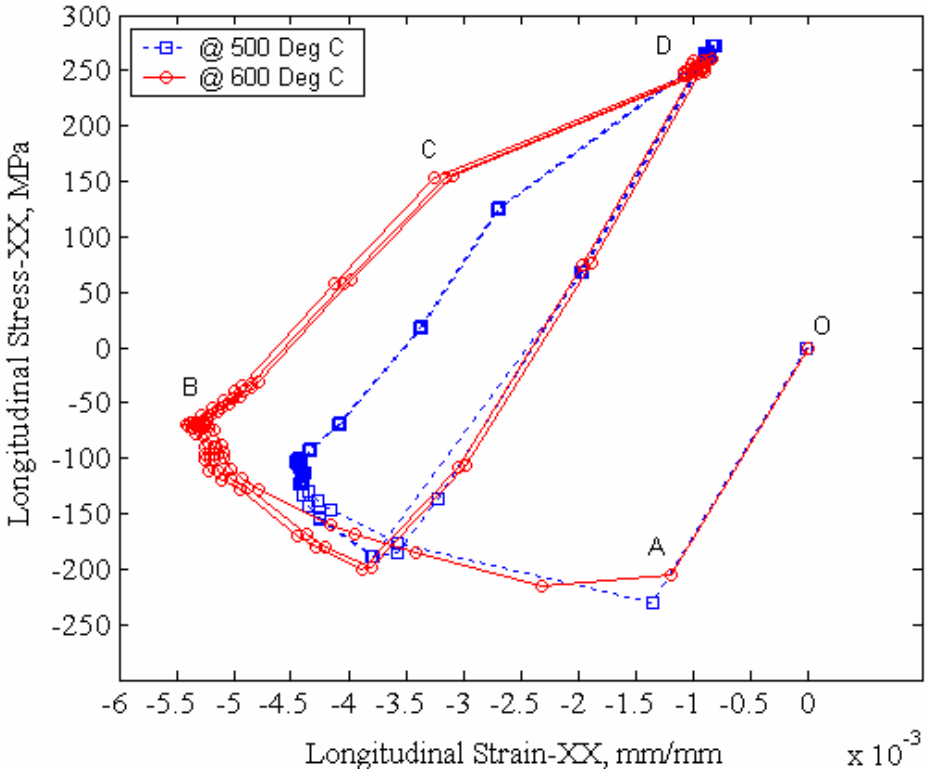

Fig. 8: Cyclic stress-strain plot from FEA results.

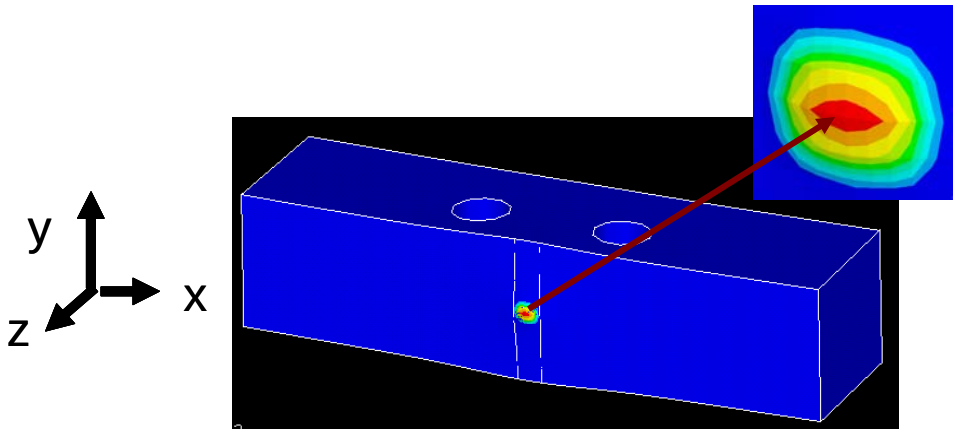

Fig. 9: Contour plot showing the localized plastic strain in the x-direction at 600 ºC (Sample A).

4. Selection of Fatigue Life Prediction Model

Fatigue damage is defined as a progressive, localized, and permanent structural change that occurs in a material subjected to cyclic stresses and strains that may culminate in cracks or complete fracture after a finite number of cycles [9]. Over the years, extensive research work has been carried out to understand the different phases of the fatigue phenomenon and thus quantify different phases of fatigue damage in terms of fatigue life. The four distinct phases of fatigue are: (a) nucleation of microcracks of the order 0.1 μm-1 μm [10], (b) propagation and coalescence of the microcracks to form small cracks of easily definable length in the 0.5-mm to 1-mm range [10], (c) propagation of the small cracks until the fracture toughness of the material is exceeded, and (d) final instability. In the present study, thermal fatigue life is estimated as the number of thermal cycles required from the time of initiating a surface imperfection or a grain-size crack to the time an "engineering-size crack" (crack size ~ 1-1.5 mm) is formed [11].

For thermal fatigue life prediction, the strain-based approach is considered to be the most appropriate. Most of the strain-based fatigue life prediction models at elevated temperatures are based on the well-known Coffin-Manson model [12] proposed independently by Coffin and Manson in 1954. This model postulates that for low-cycle fatigue conditions where the material has undergone a significant amount of inelastic deformation, the fatigue life is related to the imposed range of the inelastic strain by

$$\frac{\Delta\varepsilon_p}{2} = \varepsilon_f \left(N_f\right)^c, \tag{2}$$

where $\frac{\Delta\varepsilon_p}{2}$ is the plastic strain amplitude, ε_f is the fatigue ductility coefficient, c is the fatigue ductility exponent, and N_f is fatigue crack initiation life. Since many applications fall under the category of intermediate fatigue conditions, where both elastic and plastic strains are equally significant, Eq. (2) was modified to include the elastic strain amplitude. It was shown by Manson [13] that the fatigue resistance of a material could be characterized by

$$\frac{\Delta\varepsilon_{total}}{2} = \frac{\sigma_f}{E}\left(N_f\right)^b + \varepsilon_f \left(N_f\right)^c \tag{3}$$

where $\frac{\Delta\varepsilon_{total}}{2}$ is the total strain amplitude, σ_f is the fatigue strength coefficient, E is the Young's modulus of the material, b is the fatigue strength exponent, and N_f is fatigue crack initiation life. While Eq. (3) has been widely used for correlating uniaxial strain-controlled fatigue test data for a wide range of materials, this equation is not adequate for predicting fatigue life at elevated temperatures.

Selection of an appropriate fatigue life prediction needs to be based on the following considerations: (a) multi-axial stress state in the material, and (b) hold-time effect. Hold time, during which the material may be under peak stress for a prolonged period during each cycle, can significantly lower the estimated fatigue life [14,15]. In recent years a number of approaches have been proposed to extend Eq. (3) to multi-axial loading conditions and also to incorporate the effect of mean stress that is induced as result of creep/stress occurring during hold time.

One such approach that provides good fatigue life prediction for a material that fails in a tensile manner is the Socie-modified Smith-Watson-Topper model [16]. It can be used for in-phase multi-axial loading conditions (in which the different components of the stress tensor at a given material point in the solid vary in constant proportion to one another). This model postulates that a crack would grow perpendicular to the maximum tensile stress, and the parameters that control damage are the maximum

principal strain amplitude and the maximum principal stress on the maximum principal strain plane. The fatigue life is predicted by

$$\frac{\Delta\varepsilon_l}{2}\sigma_{\max} = \frac{(\sigma_f)^2}{E}(2N_f)^{2b} + \sigma_f \varepsilon_f (2N_f)^{b+c}, \tag{4}$$

where $\frac{\Delta\varepsilon_l}{2}$ is the maximum principal strain range, and σ_{max} is the maximum stress on the maximum principal strain plane. The parameters on the right-hand side are defined as in Eq. (3). It can be stated that Eq. (4) also contains the influence of mean stress based on the following identity:

$$\sigma_{\max} = \sigma_m + \frac{\Delta\sigma}{2}, \tag{5}$$

where σ_m is the mean stress, and $\Delta\sigma$ is the stress range.

5. Fatigue Life Estimation—Results and Conclusions

The parameters ε_f, σ_f, b, and c in Eqs. (3)-(5), defined as material properties, were obtained from the monotonic tensile stress strain data at room temperature using the empirical equations [8] given below.

$$\varepsilon_f = -\ln(1 - R.A), \tag{6}$$

where *R.A* is the percentage reduction in area. For Glidcop Al-15 the value of *R.A* is ~ 40%. For calculating the fracture strength σ_f, the average fracture stress σ_{avg} was first computed using the empirical formula

$$\sigma_{avg} = -\sigma_u (1 + R.A), \tag{7}$$

where σ_u is the ultimate tensile strength. For Glidcop Al-15, this value is 385 MPa. The fracture strength σ_f is then obtained by correcting for necking using the Bridgeman's equation

$$\sigma_f = \frac{\sigma_{avg}}{\left(\left(1 + \frac{2R}{r_f}\right)\left(\ln\left(1 + \frac{r_f}{2R}\right)\right)\right)}, \tag{8}$$

where

$$\frac{r_f}{R} = 0.76 - 0.94(1 - \varepsilon_f). \tag{9}$$

The parameter fatigue strength exponent *b* is calculated using

$$b = \frac{-n'}{(1 + 5n')}, \tag{10}$$

where n' is the cyclic strain hardening exponent. For Glidcop Al-15 the average value of the strain hardening exponent is ~ 0.15 [17]. A value of –0.6 for fatigue ductility exponent *c* was obtained from

the literature [7]. The values of the fatigue material constants for Glidcop Al-15 are summarized in Table 4.

Table 4: Material Properties of Glidcop Al-15 for Fatigue Life Prediction

Parameter	**Value**
Reduction in area, %	40
Ultimate tensile strength, MPa	385
Fatigue ductility coefficient, ε_f	0.5
Fatigue strength coefficient, σ_f	503
Fatigue ductility exponent, c	–0.6
Fatigue strength exponent, b	–0.085

A Matlab® program was written for postprocessing the stress and strain values obtained from the finite element analyses. Fatigue life estimates were obtained for the ESRF test samples using Eq. (5) by an iterative procedure. The results, shown in Table 5, predict fatigue life of 22,600 cycles at 500 °C, and 13,000 cycles at 600 °C. As shown in Fig. 2, extensive surface cracks and a deeper crack of ~ 1 mm was observed in the test samples cycled at the peak temperature of 600 °C. Based on this comparison, the Socie-modified Smith-Watson-Topper model appears to give reasonably good estimates of the thermal fatigue life of Glidcop Al-15.

Table 5: Fatigue Life Estimates

	@500 ºC with no hold time	**@600 ºC with no hold time**
Maximum stress , σ_{max} (MPa)	272.37	263.24
Strain amplitude, $\frac{\Delta\varepsilon_l}{2}$ (mm/mm)	0.0018	0.0022
Life, cycles	22,600	13,000

In the ongoing thermal fatigue experiment at APS, all four samples will be subjected to a cycle count of 10,000 cycles but with different peak temperatures. After the completion of the thermal cycling, a detailed optical microscopy study will be carried out on all the specimens for investigating fracture patterns such as crack depth, crack orientation, fracture modes, etc.

6. Preliminary Hold Time Study

In the numerical simulations explained in the previous sections, the effects of hold time and strain rate were neglected for the sake of simplicity. Ostergren [14], who investigated the effect of hold time on the low-cycle fatigue life of several metals, has shown by means of the cyclic stress strain curves that during the hold time, stress relaxation occurs due to creep phenomenon. This in turn develops a biased stress opposite to the hold direction, thus leading to a mean stress. This mean stress coupled with increased inelastic strain, as shown in Fig. 10, causes a reduction in the fatigue life.

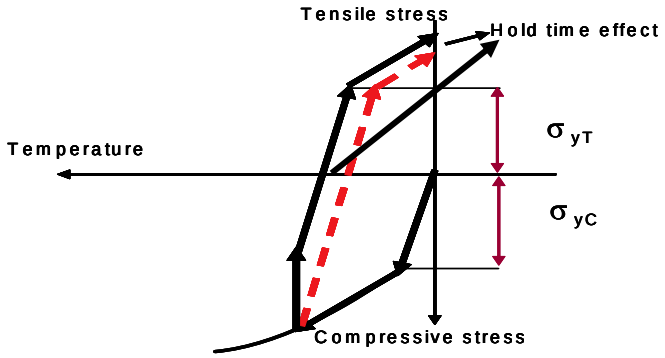

Fig. 10: Effect of hold time; creep and stress relaxation.

In order to investigate the effect of hold time on fatigue life, a preliminary numerical analysis was carried out in which a secondary "Norton"-type equation was used to model the creep behavior of Glidcop Al-15. This equation is expressed as

$$\dot{\varepsilon}_{cr} = C_1 \sigma^{C_2} \exp\left(-\frac{C_3}{T}\right), \tag{11}$$

where $\dot{\varepsilon}_{cr}$ is the steady-state creep rate, σ is the stress value in MPa, T is the absolute temperature, and C_1, C_2, and C_3 are material constants. For Glidcop Al-15, C_1, C_2, and C_3 are 1.9928E-19, 11.56, and 23706, respectively [18]. The results of this analysis are shown in Fig. 11 by the black dashed curve. Also shown for a comparison is the hysteresis plot at 600 ºC without the hold-time effect.

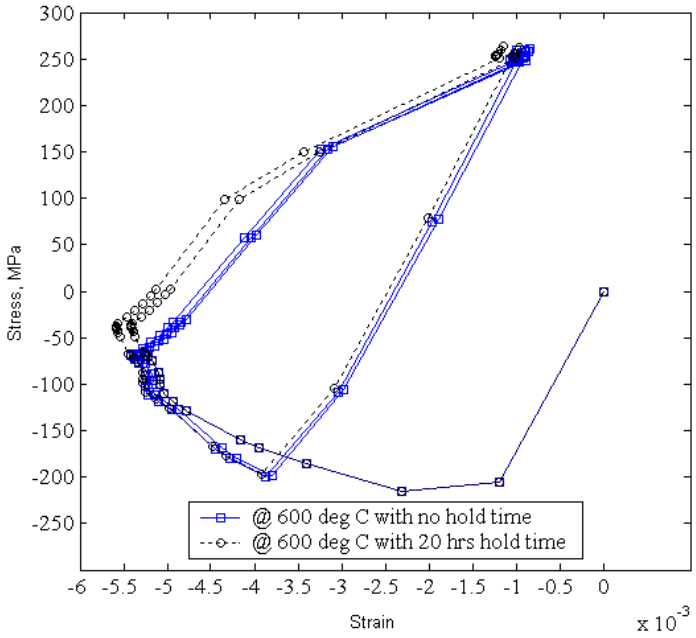

Fig. 11: Cyclic stress-strain plot from FEA results; effect of hold time.

Using Eq. (5), the fatigue life for the case with 20 hours of hold time was estimated to be 10,325. From the result of this preliminary analysis, it appears that a dwell/hold time of 20 hours at 600 ºC can reduce the fatigue life of Glidcop Al-15 by at least 20%.

Future work will be aimed at completing the thermal cycles on the APS samples and determining crack propagation through the samples by micrographs. Additionally, the fatigue life prediction will be further refined by including better creep and stress-relaxation models in the finite element analysis.

7. Conclusions

The following conclusions can be drawn from the fatigue experiments carried out at ESRF and APS:

1) Experimental and analytical results at ESRF and APS indicate that the present conservative design guidelines for Glidcop high-heat-load components are too conservative for low-cycle fatigue and should be relaxed substantially.

2) Elasto-plastic FEA models (with temperature-dependent material properties) can be used as tools for understanding the evolution of temperature and stress-strain fields under multi-axial loading situations.

3) A Socie-modified Smith-Watson-Topper model appears to give reasonable thermal fatigue life estimates for Glidcop.

4) Based on a secondary creep model, hold time (beam on for long durations) can have an appreciable effect on the thermal fatigue of Glidcop.

8. Acknowledgments

The authors are grateful to the staff of the 26-ID beamline at APS, J. Maser, B. Stephenson and R. Winarksi, for their generous support. Thanks are also due to R. Dortwegt, C. Putnam, and M. Bracken for technical support in the beamline hutch, and to Cathy Eyberger for editing the paper.

The work at Argonne was supported by the U.S. Department of Energy, Office of Science, Office of Basic Energy Sciences, under Contract W-31-109-ENG-38.

9. References

[1] S. Sharma, E. Rotela and A. Barcikowski, "High Heat –Load Absorbers for the APS Storage Ring," MEDSI 2000 proceedings, 2000.
[2] L. Zhang, J. C. Biasci, S. Sharma, V. Ravindranath, B. Rusthoven, "Thermal Fatigue of Glidcop with Undulators Power," these proceedings.
[3] R.J. Dejus, I.B. Vasserman, S. Sasaki and E.R. Moog, "Undulator A Magnetic Properties and Spectral Performance," ANL/APS/TB-45, May 2002.
[4] Verbal communication with R.J. Dejus.
[5] "ANSYS Elements Reference," Release 10.0 documentation for ANSYS.
[6] OMG Americas Corp., "Glidcop Dispersion Strengthened Copper, Glidcop Al-15 (C15715)," Technical Data Sheet, August 1989.
[7] J. Robles, K.R. Anderson, J.R. Groza, J.C. Gibeling, "Low-Cycle Fatigue of Dispersion-Strengthened Copper," Metall. Mater. Trans. A 25A (Oct 1994) 2235.
[8] M.R. Mitchell, "Fundamentals of Modern Fatigue Analysis for Design," ASM Handbook–Fatigue and Fracture, v. 19, pp. 227-249.
[9] M.E. Fine and Y.W. Chung, "Fatigue Failure in Metals," ASM Handbook–Fatigue and Fracture, v. 19, pp. 63-72.
[10] P. Lukas, "Fatigue Crack Nucleation and Microstructure," ASM Handbook–Fatigue and Fracture, v. 19, pp. 96-109.
[11] Y. Murakami, K.J. Miller, "What is Fatigue Damage? A View Point from the Observation of Low Cycle Fatigue Process," Int. J. Fatigue 27, (2005) 991.
[12] L.F. Coffin, "A Study of the Effects of Cyclic Thermal Stresses on a Ductile Metal," T. ASME 76 (1954) 931.

[13] S.S. Manson, *Thermal Stress and Low Cycle Fatigue*, (McGraw-Hill: New York) 1966, ISBN #65-25918.
[14] W.J. Ostergren, "Damage Function and Associated Failure Equations for Predicting Hold Time and Frequency Effects in Elevated Temperature, Low Cycle Fatigue," J. Test. Eval. 4 (Sept 1976) 327.
[15] C.E. Jaske, H. Mindlin and J.S. Perrin, "Influence of Hold-time and Temperature on the Low-Cycle Fatigue of Incoloy 800," J. Eng. Ind. 94 (1972) 930.
[16] A. Fatemi, D.F. Socie, "A Critical Plane Approach to Multiaxial Fatigue damage including out-of-phase loading," Fatigue Fract. Eng. M. 11 (1988) 149.
[17] T.S. Srivatsan, S. Anand and J.D. Troxell, "High Strain Cyclic Fatigue and Fracture of an Oxide Dispersion Strengthened Copper Alloy," Eng. Fract. Mech. 46 (1993) 183.
[18] J.J. Stephen and D.T. Schmale, "Mechanical Properties of Dispersion Strengthened Copper: A Comparison of braze cycle annealed and coarse grain microstructrures," Sandia National Laboratories Report No. SAND87-1351, 1987.